# Synthesis of Novel Nanocomposite CaO/AC/ZnO from Biogenic Wastes of Date Palm Seeds from The Najran Region (Saudi Arabia) and Eggshells for Degradation of Methylene Blue

NABIL A. ALHEMIARY[1,2]

[1]*Department of Chemistry, College of Science and Arts- Sharourah, Najran University, Sharourah, Saudi Arabia*.

[2]*Department of Chemistry, College of Science, Ibb University, P. O. Box 70270, Ibb, Yemen.*

*Author for correspondence. E-mail*: dralhemiary@gmail.com

**Abstract:** Metal nanoparticles and activated carbon-based nanocomposite materials are gaining popularity due to their numerous potential applications in a wide range of materials science areas. The current study aims to create novel photocatalyst frameworks for nanocomposites that were synthesized from biogenic waste and used to photodegrade methylene blue (MB) in wastewater under visible light. The activated carbon from date seeds was calcinated at a temperature of 700°C for two hours, and its surface was improved using zinc oxide nanoparticles and calcium oxide nanoparticles manufactured from eggshells at 900oC. XRD, FT-IR, SEM, BET, and TEM analyses were used to characterize the produced nanocomposites. The synthesized nanocomposite photocatalytic activity was evaluated by degrading MB dyes, its model of water pollution. The results showed that the nanocomposite CaO/AC/ZnO has a mesoporous structure with great sorption capability. Also, the photodegradation efficiency of MB using AC, CaO, AC/ZnO, and CaO/AC/ZnO nanocomposite was 33.23, 37.58, 54.61, and 88.92%, respectively, after100 min of sunlight irradiation indicating that photodegradation efficiency increases by improving the surface properties of AC. The CaO/AC/ZnO nanocomposite exhibited a 96.7% removal efficiency of MB following 120 min of visible light radiation exposure. Therefore, the CaO/AC/ZnO nanocomposite has a promising opportunity to function as a versatile and effective photocatalyst for photodegradation of organic dyes in wastewater.

**Keywords:** Date Seed Activated Carbon; Nanocomposite Materials; Photodegradation, Methylene Blue.

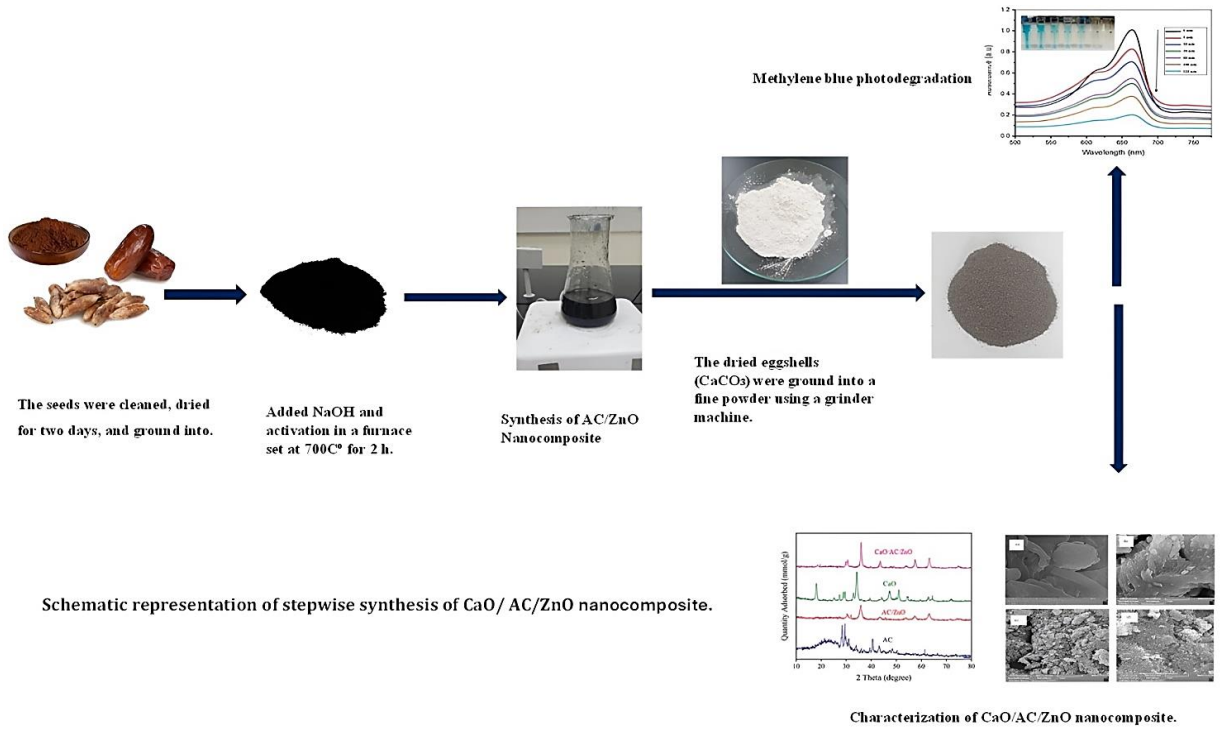


Schematic representation of stepwise synthesis of CaO/ AC/ZnO nanocomposite.

Characterization of CaO/AC/ZnO nanocomposite.

## 1. INTRODUCTION

Water pollution is a problem in many industrialized and developing nations because of the discharge of leftover organic compounds or dyes. The health of humans is seriously threatened by drinking water tainted with dyes; thus, it must be treated before consumption. Adsorption technology offers several advantages over other

technologies for treating wastewater, including simplicity of handling, speed and affordability [1].

One popular cationic dye that may create a stable solution with water at room temperature is methylene blue (MB) [2]. MB which is frequently used to color cotton, silk, wool and paper, is one of the ingredients that the dye industry uses the most [3]. Blue methylene due to its severe toxicity, if the concentration increases to a certain level[4], it causes health risks to humans, such as blindness, stomach and intestinal disease[3]. In addition, it results in methemoglobinemia, diarrhea, cyanosis, gastritis, jaundice, shock, irritation of the skin and eyes, tissue necrosis and vomiting [5]. Furthermore, sewage treatment is a pressing topic because nearly all dyes are resistant to environmental factors and difficult to biodegrade. The development of efficient and affordable materials to eliminate MB and other colors from wastewater and restore the ecosystem is therefore very crucial [2]. MB dye has detrimental effects on water quality, hence treating wastewater containing it before releasing it into the environment is crucial [2]. To extract MB and other textile colors from industrial effluent, scientists have reported using a variety of techniques. Adsorption [6], biosorption [7], nanofiltration [8][9], vacuum membrane distillation[10], phytoremediation [11][12], ultrafiltration [13], biodegradation [14], electrocoagulation [15], coagulation [16], microwave treatment[17], and liquid-liquid extraction [18]. It is difficult to break down MB dye into smaller inorganic molecules using standard techniques because of its heat and light stability as well as non-biodegradability [19]. Each of these treatment modalities has advantages and disadvantages in terms of cost and practicality, effectiveness, and environmental impact. [3][17].

Recently, advanced oxidation techniques have changed wastewater treatment methods. They break down both organic and inorganic contaminants to produce very reactive free radicals, or •OH. •OH-free radicals' potent oxidizing properties cause carbonaceous species to be converted into inorganic ions and $CO_2$ gas[4]. •OH can be formed by oxidants like hydrogen peroxide and ozone. This can be finished using homogeneous or heterogeneous photocatalysts such as ZnO [20], or with energy resources like heat, ultrasounds, and ultraviolet light[21]. The heterogeneous photocatalytic method effectively breaks down toxic substances in the environment by producing excitons when exposed to light[22] [23].

An adsorbent with the greatest potential is activated carbon (AC) and a big surface area, has high surface activity. The extremely porous structure contributes to its adsorption qualities, catalysts, and catalyst supporters are among the applications for various forms of AC[24]. In the literature, the most common substance used to extract contaminants from wastewater is activated carbon (AC). In order to produce sustainable nanohybrid composites from metallic oxide, efforts are being made to identify activated carbon alternatives [25]. Natural plant materials have been used to create nanohybrid composites in a novel way recently. These materials include leaves[26], ([27], gum [28], sprouts [29], and seeds[30] [31] [25] which are converted into biochar or activated carbon. Activated carbon may have its surface properties improved with a range of materials, Zinc oxide is among the most crucial elements for improving the surface of activated carbon [32]. In addition, CaO has a large surface area, low cost, easy synthesis, and a substantial capability for pollutant separation [33].

One of the most significant and vital foods and crops in the Arab world is the data palm fruit *(Phoenix dactylifera)*. Fruit seeds are rich in a variety of functional chemicals that are essential for nutrition, such as sugars, fatty acids, protein, fiber, ash, minerals and vitamins, in addition to significant concentrations of flavonoids and phenolic compounds [34]. There are a lot of palm trees in Saudi Arabia and plants of almost 23 million trees, the Kingdom produced 1.5 million tons of palm date fruits in 2020, which accounts for 14.4% of the global production. [35]. Date seeds comprise 6.1-11.5% of the fruit and are one of the primary waste products and constitutes an environmental problem in Saudi Arabia [36]. Eggshells are a natural waste that can be recycled to produce nanomaterials at a low cost is to produce calcium oxide (CaO) for use in environmental applications[37].

Using activated carbon for the green synthesis of metal oxide nanoparticles presents a viable substitute for conventional chemical synthesis techniques. In this study, created activated carbon nanocomposites using date palm seeds from the Najran region (Saudi Arabia), and zinc oxide nanoparticles and calcium oxide from eggshells. The produced materials were characterized using FTIR, XRD, and TEM, studying various physical and chemical properties. By employing the produced photocatalysts in various application settings, the photodegradation of methylene blue was examined under visible light radiation.

## 2. MATERIALS AND METHODS

### 2.1 Reagents and Chemicals

The reagents utilized in this experiment are all analytical grades. The following materials were acquired from Sigma-Aldrich (USA) and Merck (Germany): zinc nitrate, methylene blue, sodium hydroxide, ammonium hydroxide, and hydrochloric acid. The pH was adjusted using 1 molar of HCl and NaOH. Every solution was made using deionized water.

### 2.2 The Composite Synthesis

#### 2.2.1 Preparation of Activated Carbon from Date Palm Seeds

The date seeds were obtained from the date palms in Najran, Saudi Arabia. After picking the fruits, the seeds were carefully cleaned with deionized water and allowed to dry for two days. The seeds were subsequently removed and ground into powder after being carbonized for 120 minutes at 400 °C in the furnace. The powder was then added to the sodium hydroxide solution for activation [38]. The activated carbon was placed in a furnace set at 700 degrees Celsius for two hours. After the powdered activated carbon was allowed to cool fully at room temperature, it was repeatedly cleaned with deionized water until its pH reached 7 and it was neutralized [39].

#### 2.2.2 Synthesis of AC/ZnO Nanocomposite

Two grams of activated carbon were added to a 250 ml beaker along with one gram of zinc nitrate that had been dissolved in 50 milliliters of deionized water. The mixture was then mechanically agitated for two hours at 240 rpm. A few drops of $NH_4OH$ were gradually added after complete homogeneity until precipitation was seen. After being washed with deionized water and centrifuged again at 6,000 rpm, the precipitate was dried at 110 $^oC$ for 2 hours, and then calcined at 550$^oC$ for three hours.

The Synthesis of CaO/AC/ZnO nanocomposite CaO nanoparticles was made using hen eggshells a natural waste. After collecting eggshells, the discarded were thoroughly washed in tap water to get rid of any dirt, pollutants, and organic materials that had attached to the surface. They were then cleaned once more with distilled water numerous times. The previously washed eggshells were then dried in a 150°C oven for three hours to remove the water. The dried eggshells were ground into a fine powder using a grinder machine [40]. To get the finest eggshell powder, the fine eggshell powder was put through a sieve with a mesh size of 100 µm. 2g of eggshell powder was added to water to deposit calcium oxide on the nanocomposite's surface. Eggshell powder is insoluble in water, and the resulting solution is heterogeneous. Then 1g of nanocomposite (AC/ZnO) was added, and the mixture was agitated using a magnetic stirrer for one hour. Then, it was heated to 900$^oC$ in the furnace to turn the $CaCO_3$ into CaO[41].

### 2.3 Methylene blue (MB) Solution Preparation

One gram of MB was dissolved in one liter of deionized water to create a 1000 mg/L MB solution. Subsequently, MB concentrations were created by serial dilution.

#### 2.3.1 Evaluation of Photocatalytic Activity

This study examined the photocatalytic performance of synthesized materials' CaO, AC/ZnO and CaO/AC/ZnO nanocomposite photocatalysts under visible light from a 100 W incandescent light bulb at 15 cm. The results indicated that showed that MB removal was achieved by CaO, AC/ZnO, and CaO/AC/ZnO nanocomposite of parameters effects of pH, photocatalyst amount, MB concentration, and time of irradiation. To initiate the degradation experiment, transfer 100 mL of the MB aqueous solution (10 mg/l) into a 250 mL conical flask, then add 50 mg of the nanocomposite. The pH of the solutions was adjusted using 0.1 M NaOH and 0.1 M HCl solutions. The samples were centrifuged for 10 minutes at 4,000 rpm, and then they were filtered. After that, the filtrate was tested to check if the MB concentration had changed using a UV/visible spectrophotometer that was calibrated to the λmax of 665 nm shown in Figure 1. To calculate the amount of MB eliminated, equations

(1) and (2) were applied [42]:

$$\%\ \text{degradation} = \frac{C_o - C}{C_0} \quad (1)$$

Where $C_0$ represents the initial concentration of MB and C is the concentration of MB (mg/L). The effect of the time of light irradiation on the ratio of MB concentration ($C/C_0$). The starting and time truncated concentrations of MB in the aqueous phase are denoted by C and $C_0$, respectively. The $C/C_0$ ratio provides a useful visual assessment of the composite's photocatalytic activity. Photocatalytic processes have pseudo first order kinetics based on the Langmuir–Hinshelwood model [43]. The following formula may be applied to get the first order rate constant k.

$$-\ln\frac{C}{C_o} = kt \quad (2)$$

### 2.4. Characterization of CaO/AC/ZnO Nanocomposite

Fourier Transform Infrared (FT-IR) spectra were obtained using the KBr method, with a resolution of 4 cm−1 and a scan rate of 0.75 Hz. The spectra were examined across the whole spectrum range of 4000–400 cm-1 (Bruker, Ettlingen, Germany). UV-vis spectra were recorded throughout a 200–800 nm spectral range using (Thermo Fisher Scientific, Waltham, MA, USA). We scanned the crystalline phases of the AC, CaO, AC/ZnO, and CaO/AC/ZnO nanocomposite using Rigaku D/Max-2550 X-ray diffraction (λ = 0.154 18 nm). The exterior layout and dimensions have been studied using energy-dispersive X-ray (EDX) and field emission scanning electron microscopy (FESEM) from SHIMADZU Japan (SSX-550). Transmission electron microscopy (TEM) (H-7650, Hitachi, Japan) was used to analyze the microscopic characteristics and crystalline pattern of the composite. Brunauer-Emmett-Teller (BET) analysis was used to determine the specific surface area and pore volume of AC, CaO, AC/ZnO, and CaO/AC/ZnO.

## 3. RESULTS AND DISCUSSION

### 3.1 FT-IR spectroscopy Analysis

FT-IR analysis can be a useful method for figuring out the structural properties of unknown compounds by identifying the functional groups that absorb infrared light. The functional groups in the structures of the AC, AC/ZnO, and CaO/AC/ZnO nanocomposite were determined by FT-IR analysis; the results are shown in Figure 1. The O-H and hydrogen bonds in the structure of the AC are responsible for the sorption peaks that were found at 3,742, 616, and 3,436 $cm^{-1}$, as can be shown. Additional peaks that correspond to the C=C bonds of aromatic and alkene were also seen at 1,538, 1,638, and 1,694 $cm^{-1}$ [44]. The sorption peaks located at 3,742, 3,615, and 3,436 cm-1 in the AC structure were shifted to 3,848, 3,743, and 3,424 $cm^{-1}$ in the AC/ZnO structure respectively. The peaks at 1,538, 1,638, and 1,692 $cm^{-1}$ were transferred to 1,536, 1,620, and 1,697 $cm^{-1}$ respectively. The presence of ZnO nanoparticles in the structure of the specified composites is confirmed by a significant sorption peak that emerged at 546 $cm^{-1}$, which is attributable to the ZnO vibrations [45], [46]. The structure of CaO exhibited a high adsorption peak at 3,646 cm-1, which may be related to the hydroxyl groups' OH bond (Ca-OH). Broad adsorption peaks were seen at 1,474 and 1,421, $cm^{-1}$; these values suggest that the CaO structure contains both mono and pair carbonates[47][12]. The CaO/AC/ZnO nanocomposite's synthesis resulted in the observation of sorption peaks in the CaO structure although with marginal variations in intensity. Peaks at 574 and 876 $cm^{-1}$, for instance, were moved to 570 and 871 $cm^{-1}$, respectively, and peaks at 1,420 and 1,472 $cm^{-1}$ were relocated to 1,419 and 1,513 $cm^{-1}$. Additionally, two peaks in the CaO/AC/ZnO structure were detected at 3,400 and 3,800 $cm^{-1}$. These peaks show that ZnO and calcium oxide have been found in the activated carbon structure and that the CaO/AC/ZnO nanocomposite is well-constituted.

### 3.2 XRD Analysis

X-ray diffraction (XRD) is a practical and effective method for verifying the identification of the expected components present in prepared nanoparticle samples [48]. Figure 2 shows the results of an XRD examination

that was conducted to investigate the crystal structures of the AC, AC/ZnO, and CaO/AC/ZnO in the 10 to 80° range. The results indicate that the structures of AC, AC/ZnO, and CaO/AC/ZnO include a few peaks with varying intensities, indicating the presence of crystalline and semi-crystalline phases. It follows that all the materials listed have a crystalline structure. Some peaks in the AC structure were found at 2θ of 20.20, 24 and 43.8°; they are connected to the graphite structure and are assigned to the crystalline phases of (002), (100) and (001) [49]. Additional peaks associated with the crystalline phases of (220), (311), (222) and (440) were found at 29.38, 36.14, 40.56 and 64.86°, respectively [50]. The reverse cubic spinel-type ZnO nanoparticles generated in the AC are indicated by several peaks in the structure of the AC/ZnO nanocomposite, which were detected at 35.84, 45.29, and 63.24°. These peaks are ascribed to the crystalline phases of (101), (102) and (440), respectively [49]. Furthermore, many peaks that had been seen in the calcium oxide structure in earlier studies were observed at 2θ of 18.35, 33.94, 34.39, 39.84, and 54.36° in the XRD study for CaO. Furthermore, distinct peaks were detected at 2θ of 18.81, 29.68, 34.29, 35.82, 43.49, 53.99, and 63.28° in the CaO/AC/ZnO nanocomposite structure. These peaks signify the existence of CaO in the AC/ZnO composite structure and the creation of the CaO/AC/ZnO nanocomposite[51].

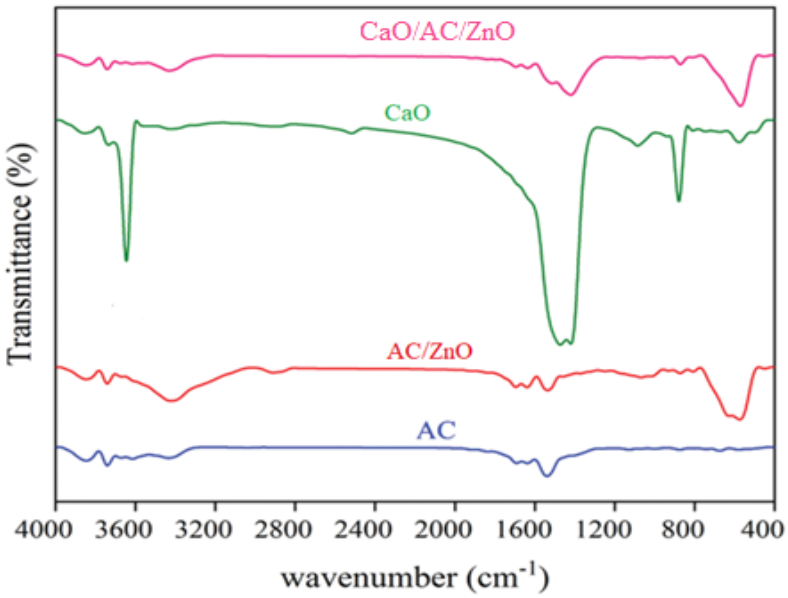


**Figure 1.** The results are FT-IR spectra of AC, AC/ZnO, CaO, and CaO/AC/ZnO.

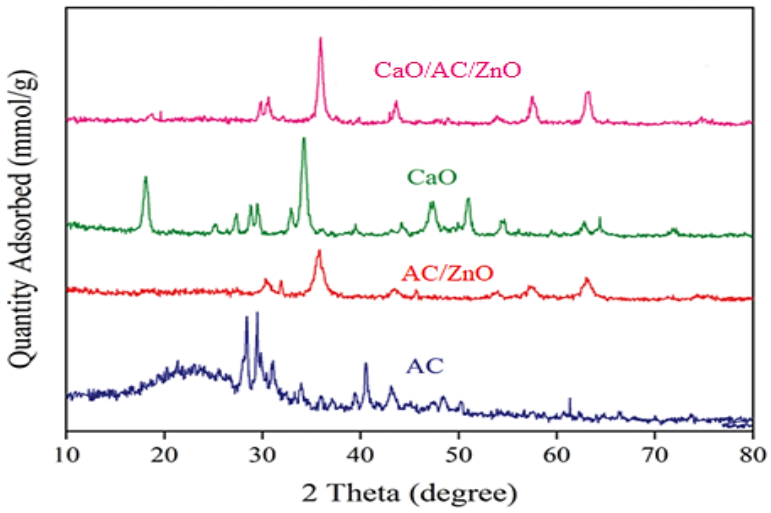


**Figure 2**. The results XRD analysis for AC, AC/ZnO, CaO, and CaO/AC/ZnO.

### 3.3 SEM and TEM Analysis

SEM analysis was utilized to investigate the surface morphology of the AC, CaO, AC/ZnO, and CaO/AC/ZnO composites structures. The results are displayed in Figure 3. It is evident that the date seed-based activated carbon has a porous and flat surface figure 3 (a). Following the implantation of ZnO nanoparticles on the AC surface, a few particles of varying sizes are seen. These particles may arise from the ZnO nanoparticles' creation on AC surface, causing surface irregularities and alterations show in figure 3 (b). CaO structure has a large number of pores, as figure 3(c) of the SEM examination illustrates [52]. Also, the surface morphology of the CaO/AC/ZnO nanocomposite has layered structures, high porosity, and surface unevenness, all of which can be advantageous for the absorption of various pollutants, as seen in figure 3(d).

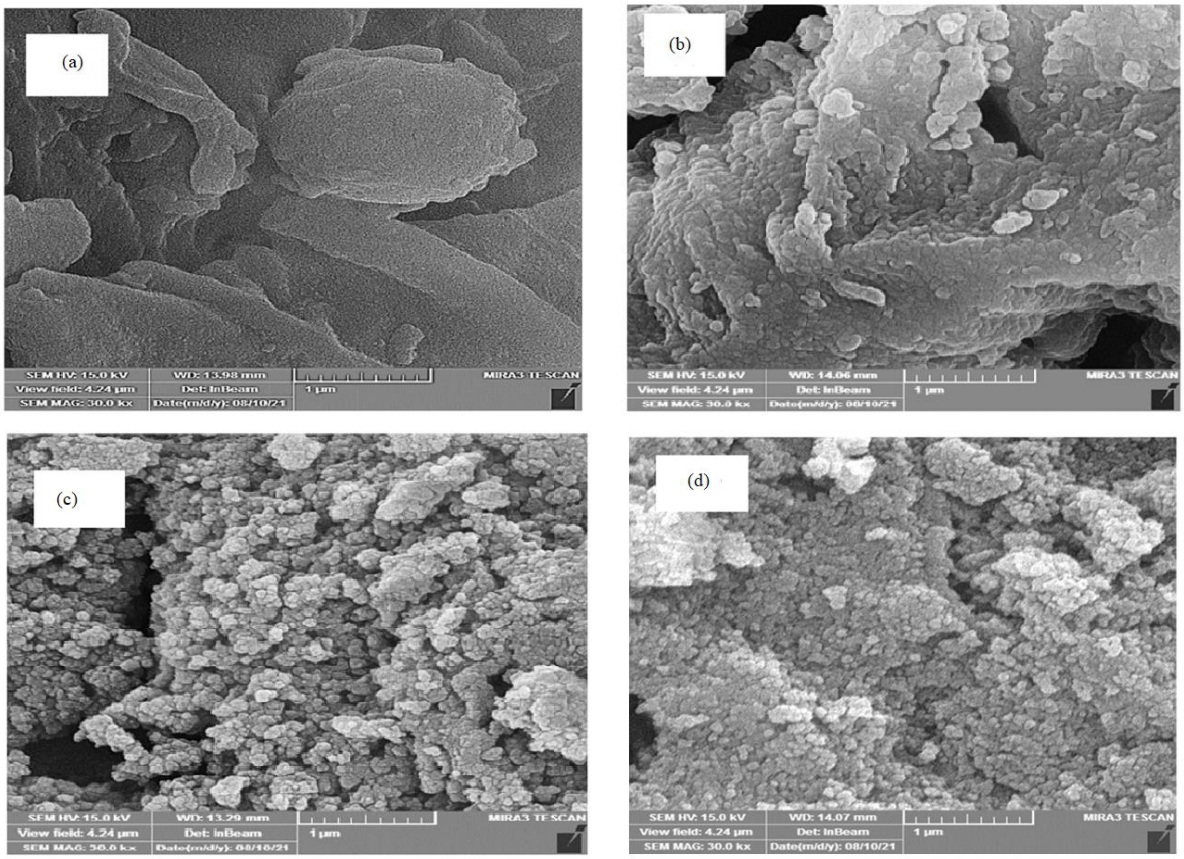


**Figure. 3**. The results of SEM analysis for (a) Ac, (b) CaO, (C) AC/ZnO, and (d) CaO/AC/ZnO.

The morphology and structure of the date seed-derived AC, CaO, AC/ZnO and CaO/AC/ZnO nanocomposite were examined using TEM analysis examination in figure. 4. The shape of the AC/ZnO composite, as depicted in Figure. 4(b), demonstrates that ZnO nanoparticles with a spherical structure are successfully distributed on the AC surface and interact appropriately [49]. The outcomes showed that ZnO nanoparticles, AC, and CaO were present in the composite structure after the production of the CaO/AC/ZnO nanocomposite Figure. 4(d), which is consistent with the findings of the SEM examination.

Table 1 shows the Brunauer-Emmett-Teller (BET) findings analysis for the AC, CaO, AC/ZnO and CaO/AC/ZnO nanocomposite. Specific surface areas of 414.01, 2.502, 76.926 and 43.193 m2/g were found for the AC, CaO, AC/ZnO and CaO/AC/ZnO, respectively. The specific surface area of AC was much higher than that of the other adsorbents, whereas CaO had the lowest value of this parameter[53]. The specific surface area and pore volume are important elements in sorption process because they directly affect sorption capacity of pollutants. The average pore volume was determined to be 0.2, 0.019, 0.201 and 0.182 $cm^3/g$ for AC, CaO, AC/ZnO, and CaO/AC/ZnO, respectively. The fact that these levels work well with AC, AC/ZnO, and CaO/AC/ZnO adsorbents shows how good these sorbents are in adsorbing materials.

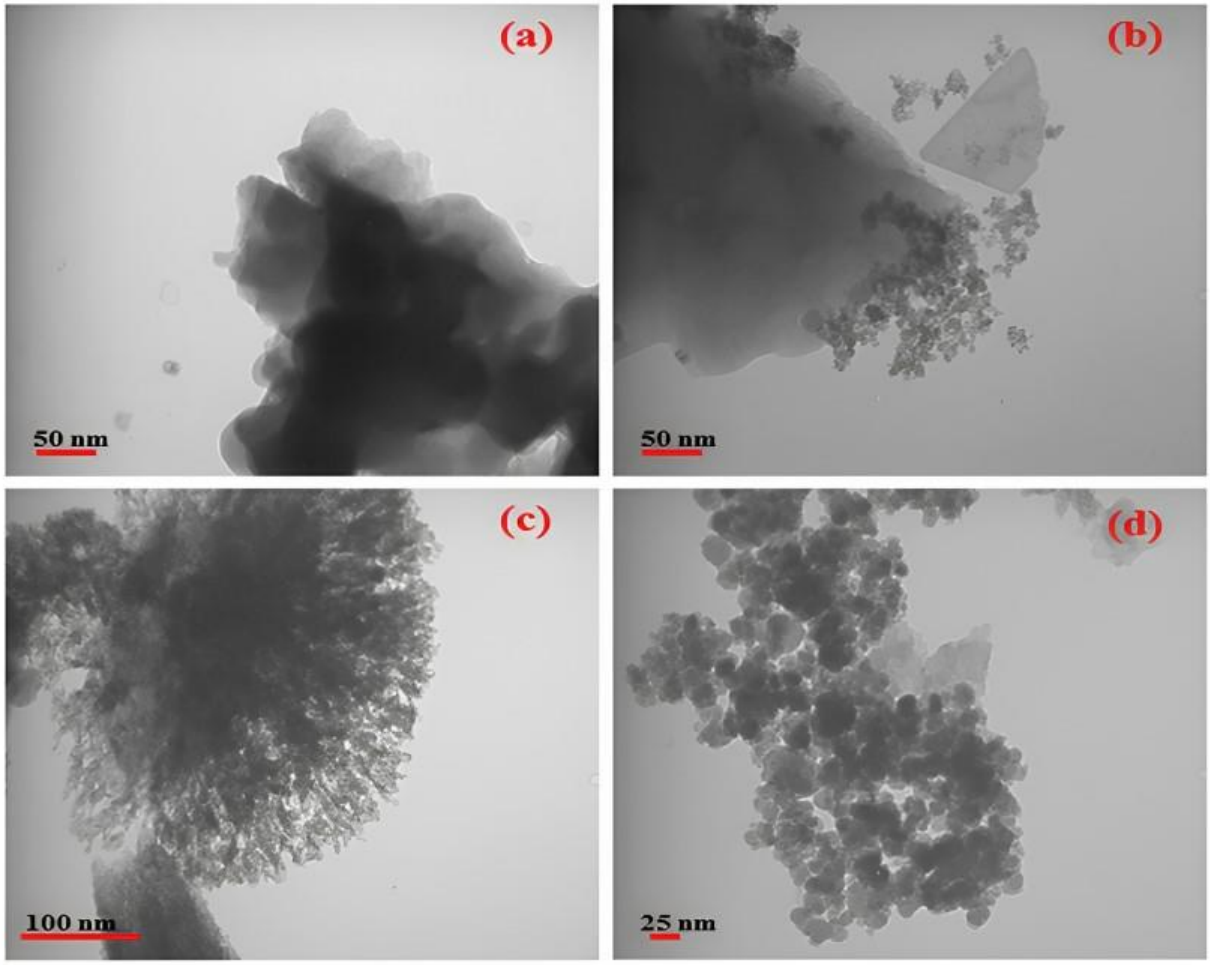


**Figure. 4 :** TEM analysis of (a) AC, (b) AC/ZnO composite, (c) CaO, and (d) CaO/AC/ZnO nanocomposite.

**Table 1. Surface characteristics of AC, CaO, AC/ZnO, and CaO/AC/ZnO**

| Parameter | AC | CaO | AC/ZnO | CaO/AC/ZnO |
|---|---|---|---|---|
| BET surface area ($m^2/g$) | 414.01 | 2.502 | 76.926 | 43.193 |
| Average Pore Volume ($cm^3/g$) | 0.2 | 0.019 | 0.201 | 0.182 |
| BJH Adsorption mean pore diameter ($^OA$) | 38.1 | 8.01 | 5.12 | 1.79 |

### 3.4 Methylene Blue Photodegradation Characteristics

#### 3.4.1 pH Effect

pH is one of the most important and practical factors in the absorption of many contaminants [3]. MB is a cationic dye that will adsorb on a photocatalyst that is substantially negatively charged [54]. The medium's pH might be adjusted to control the photodegradation of MB [55]. Lower pH (acidic fluids) causes less MB molecule adsorption on the photocatalyst surface because $H^+$, the dominant species, competes with the cationic MB dye. The interaction between •OH and MB is diminished because MB does not adsorb on the photocatalyst's surface. There is no competition between $OH^-$ and MB at higher pH levels because $OH^-$ will be repelled by the negatively charged surface of the photocatalyst and remain in the solution in large concentrations [56]. Therefore, the effect of pH on the removal effectiveness of MB from 2 to 11 was studied using CaO, AC/ZnO, and CaO/AC/ZnO nanocomposite; the results are shown in the figure. 5. There was a little change in degradation when the pH was changed from 2.0 to 7.0. The pH fell from 4.0 to 2.0, significantly reducing the efficiency of disintegration. On the other hand, more degradation was noted when the pH of the MB solution increased from 7 to 11. To achieve the maximum degradation efficiency, 120 minutes of radiation were applied. Photocatalysts with a high negative

charge are absorbed by MB since it is a cationic dye [57]. Therefore, 9 was the ideal pH for MB absorption when using the sorbents.

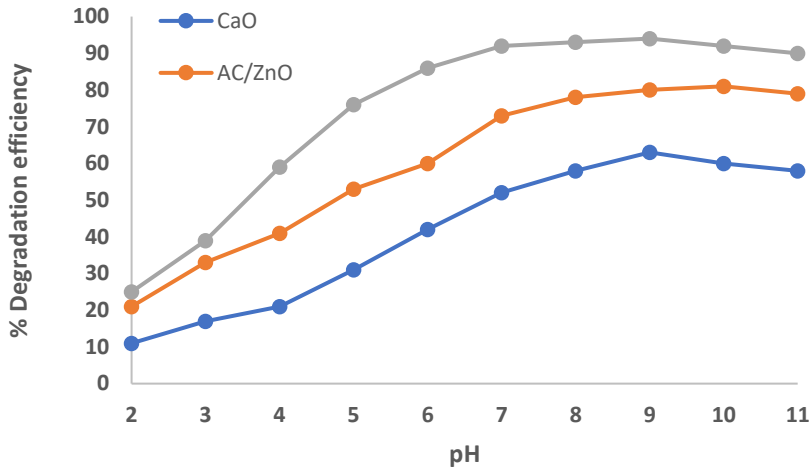


**Figure. 5.** The effect of pH on the CaO, AC/ZnO, and CaO/AC/ZnO nanocomposites ability to photodegrade MB.

### 3.4.2 Radiation Time Effect

The effect of varying irradiation times on dye degradation was investigated using MB samples under the guidance of photocatalysts, as shown in Figure 6. This work examined irradiation times effect on the MB adsorption process using the CaO, AC/ZnO, and CaO/AC/ZnO nanocomposite. The initial MB concentration was 10 mg/L, and testing was conducted at pH 9. Figure. 8(c) illustrates the findings. Due to the abundance of active sites on the adsorbent surface, it is evident that the degradation efficiency of MB employing all adsorbents increases dramatically at the start of the sorption process (almost in the first 100 min) [54]. Then, the absorption peak of MB decreases as the reaction time grows. The color shifts from blue to colorless at the same moment. The decrease in absorption spectra is due to the reduction of the MB chromophore, which results in a drop in the MB absorption peak as the reaction time rises. The color shifts from blue to colorless at the same moment. The diminution of the MB chromophore is the cause of the decline in the absorption spectra. Consequently, the photocatalysts' irradiation time was established at 100 minutes.

### 3.4.3 Effect of Concentration of MB

The initial concentration of MB is a crucial variable in the adsorption process[56], In the present work, the impact of initial MB concentration on degradation efficiency was examined using CaO, AC/ZnO, and AC/ZnO/CaO nanocomposite under optimal conditions (refer to Figure 6). The degradation efficiencies of CaO, AC/ZnO, and CaO/AC/ZnO nanocomposite decreased when the initial MB level was raised from 5 to 50 mg/L from 65.5 to 31.25%, 83.74 to 65.47%, and 96.97 to 86.89%, respectively. As a result, an MB concentration of 5 mg/L produced the greatest uptake efficiency. This reduction occurs for all adsorbents due to the saturation of active sites on the adsorbent surface at high concentrations of MB[57]. At a lower MB concentration, its absorption capacity is significant. This is because there are more active sites on the surface of the photocatalyst when the MB concentration is low [58]. At increasing MB concentrations, photodegradation is slowed down due to increased dye molecule adsorption covering the active sites of the photocatalyst. A higher concentration of dye molecules increases the light-screening effect and decreases the production of •OH active radicals [59].

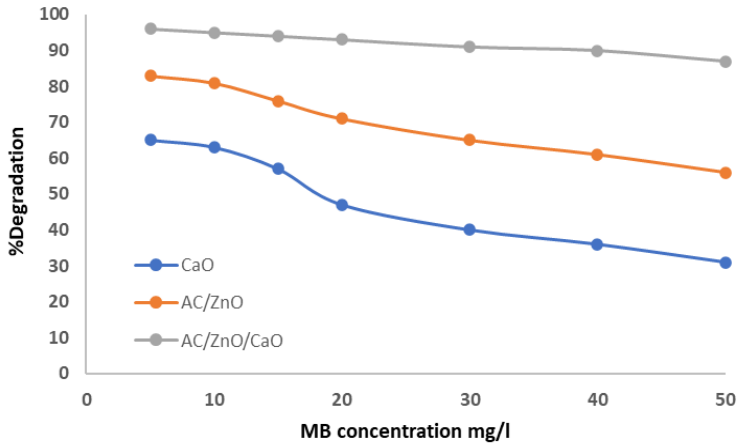


**Figure. 6.** Effect of concentration of MB versus percentage degradation through CaO, AC/ZnO, and CaO/AC/ZnO nanocomposite.

### 3.4.4 Effect of Photocatalyst Quantity

The optimum photocatalyst amount needs to be determined to achieve the greatest photodegradation of MB. The impact of catalyst loading on the photodegradation of MB was examined by subjecting CaO, AC/ZnO, and CaO/AC/ZnO composites to visible radiation while maintaining constant values for other parameters [60]. The experiment was run for 100 minutes at pH 9, starting with a 5 mg/L concentration of MB. For each liter of photocatalyst, one to four grams were utilized. The photodegradation efficiency is shown in figure 7. There is evidence to imply that the photodegradation effectiveness increased with the number of photocatalyst and sorbent active sites [61]. The photodegradation efficiency of the CaO, AC/ZnO and CaO/AC/ZnO nanocomposite rose and then remained almost constant when up to 2 g/L of photocatalyst was added. The results showed that 2.5 g/L of photocatalyst was the optimal amount for the CaO and AC/ZnO CaO/AC/ZnO nanocomposite. Agglomeration occurs when the quantity of photocatalysts is increased beyond the optimal point. The turbidity of the solution likewise increases with increasing concentration levels. These two elements reduce the efficacy of the photocatalyst by preventing photons from being absorbed on its surface [62].

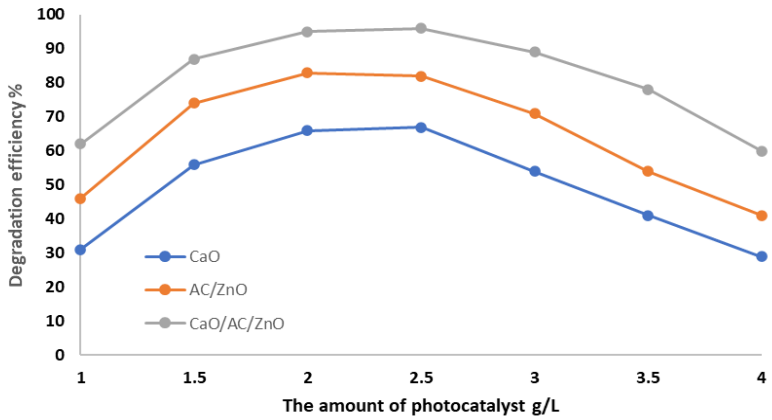


**Figure. 7.** The effect of the amount of photocatalyst on the photodegradation efficiency of methylene blue through CaO, AC/ZnO, and CaO/AC/ZnO nanocomposite.

### 3.5 Photocatalytic Degradation of Methylene Blue

The CaO/AC/ZnO composite has the highest degradation efficiency of all the adsorbents, according to the results of the examination of numerous elements of the photodegradation efficiency of the MB dye. In addition, the AC/ZnO/CaO nanocomposite showed reduced optimal values for photocatalyst amount and irradiation time during the adsorption process in comparison to the other two sorbents. The degradation efficiency with CaO was

the lowest across all experiments. The easy removal of AC from the solution is facilitated by the surface addition of CaO nanoparticles and AC/ZnO. It results in a reduction of the photocatalyst quantity and Irradiation time and increases the MB photodegradation efficiency. This means that by altering the surface of AC, the photodegradation efficiency of MB is increased and the operational expenses of the degradation process are reduced [63].

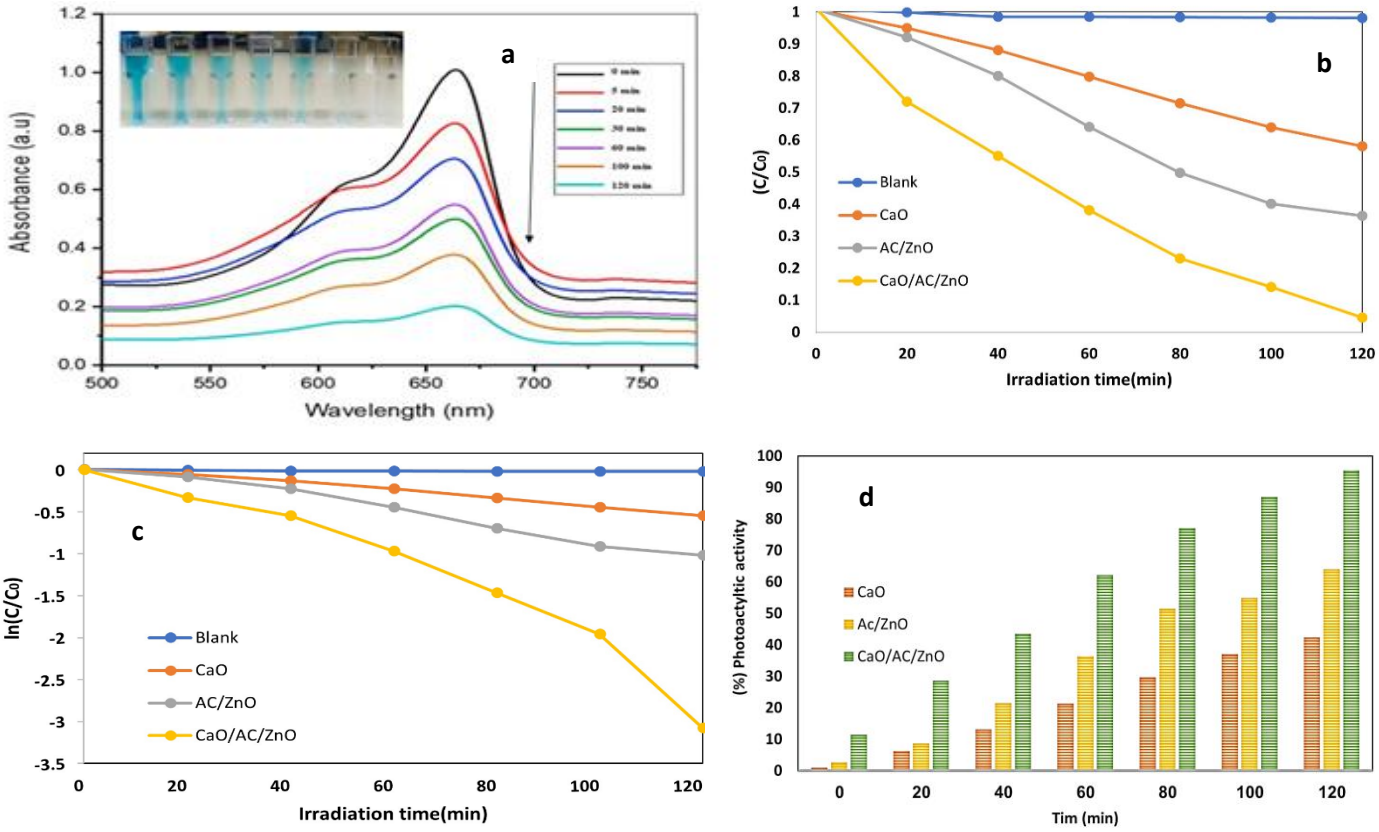


**Figure 8.** Photocatalytic degradation of composite: (a) degradation of MB at different time intervals; (b) C/C0 against time; (c) ln C/C0 against time; (d) % photodegradation efficiency.

To evaluate the photocatalytic activity of the synthesized CaO, AC/ZnO, and CaO/AC/ZnO nanocomposites, the photodegradation efficiency of MB dye under visible light radiation was employed. To find out how well the produced nanocomposites broke down the MB sample, each one was assessed identically as a function of irradiation time. The CaO/AC/ZnO photocatalyst for testing its potential has been used by applying it to colored MB dye and devastation of colored complex organic frameworks. In Figure 8(a), the absorption intensity decreases after only 100 minutes of being exposed to visible light, the peak at λ = 665 nm altered significantly, indicating the critical destructive capabilities of the CaO/AC/ZnO photocatalyst. It is widely known that the MB framework is destroyed by two methods: (i) well-defined oxidative procedures that produce base-parallel or completely flattened absorption spectra of MB molecules; (ii) a two-electron reduction process that turns colored MB into colorless leuco-MB [64]. MB was destroyed by an oxidative mechanism since, during the whole study, we were unable to observe or identify any identifiable hump at λ = 256 nm associated with the leuco-MB. The very helpful results the CaO/AC/ZnO photocatalyst produced; demonstrated the potential of this innovative photocatalytic framework for solving environmental issues. The photocatalyst with AC in the composite exhibits the highest light absorption and greatest degrading efficiency based on these findings. Figure 8(b) shows how the MB concentration ratio ($C/C^0$) is affected by the amount of time of light irradiation. Initial MB concentrations in the aqueous phase are denoted by C and $C^0$, respectively, and concentrations at time. Visually comparing the $C/C^0$ ratio is a simple method of comparing the composite's photocatalytic effect.

Photocatalytic composites produced from CaO show pseudo-first-order kinetics, as shown in Figure 8(c). The proportion of CaO and synthetic composites' degrading efficiency is displayed in Figure 8(d). Higher concentrations of AC in composites improve the photocatalyst's capacity to absorb light, which in turn boosts

photocatalytic activity, as these graphical depictions make evident. Equation one was utilized to evaluate the overall percentages of photodegradation. The sunlight at 312 nm in pure CaO shows considerable absorption[65]. The highest absorption of ZnO occurs around 367 nm. It demonstrates that ZnO is only effective in the UV spectrum [66]. Absorption can be observed in the visible to infrared spectrum for CaO, AC, and ZnO. Because activated carbon is present, the photocatalyst has a wide range of pore size configurations that allow it to absorb all visible, near-infrared, and ultraviolet radiation.

**4.6 Proposed Photochemical Reaction Mechanism.**

Scheme 1 proposes three methods to explain the photocatalytic degradation of MB dye by CaO/AC/ZnO under sunlight irradiation. The first mechanism may be explained by the fact that ZnO photocatalytic efficacy increases when exposed to visible light when AC is introduced to the photocatalytic system. This CaO/AC/ZnO combination is considered to have increased MB photocatalytic degradation efficiency. Additionally, the substantial surface area of AC may aid in the efficient adsorption of MB molecules onto the photocatalyst surface and enhance the development of π−π* interaction among the MB dye molecules. The second mechanism can result from the ZnO crystal lattice's CaO doping effect. Applying CaO doping reduces the recombination of excited electrons in the valence band (VB) with holes in the conduction band (CB). This oxidatively degradation MB molecules by producing more oxy radicals through interaction with oxygen molecules. The third mechanism may be explained by doping ZnO with CaO, which narrows ZnO's band gap. The photodegradation of MB by CaO/AC/ZnO is caused by electrochemical and reductive processes. Water molecules are oxidized by these holes into •OH. These •OH are involved in the decomposition of MB. The decomposition products of this reaction are $CO_2$ and $H_2O$. After these reactions, $•O_2$ and •OH could be generated by entrapped UV-Vis-NIR light (Equations (3)– (8). These free radicals are strong oxidizing agents and can theoretically decompose the photocatalytic degradation of MB dye.

$$CaO/Ac/ZnO + hv \rightarrow CaO/AC/ZnO(h^+_{VB} + e^-_{CB}) \quad (3)$$

$$2h^+_{VB} + 2H_2O \rightarrow 2H^+ + 2OH^{\cdot} \quad (4)$$

$$2e^-_{CB} + O_2 \rightarrow \dot{O}_2^- \quad (5)$$

$$MB* + CaO/AC/ZnO \rightarrow MB^{*+}e^-_{CB}CaO/AC/ZnO \quad (6)$$

$$MB^{*+} + OH^- \rightarrow CO_2 + H_2O \quad (7)$$

$$MB^{*+} + \dot{O}_2^- \rightarrow CO_2 + H_2O \quad (8)$$

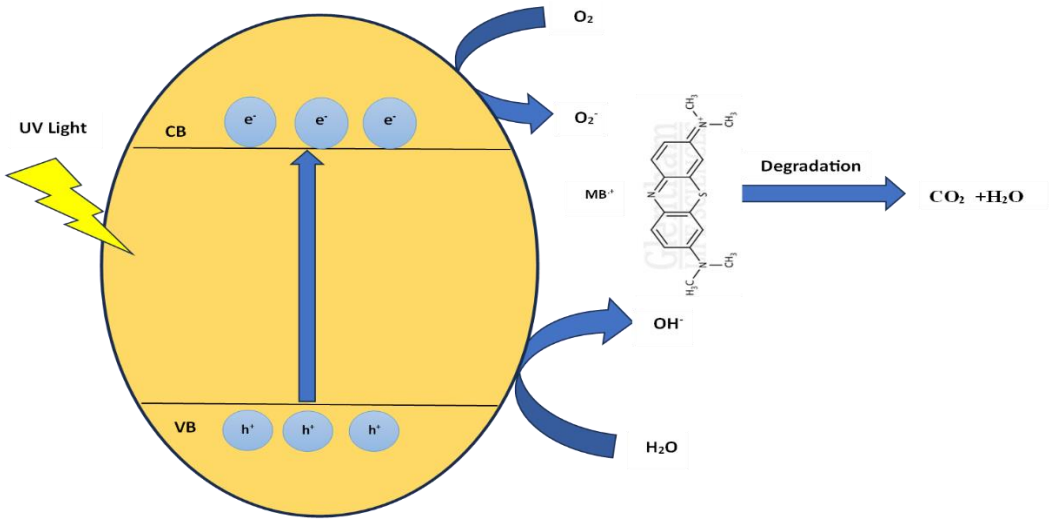


**Scheme 1**: Shows the potential process for the photocatalytic degradation of MB dye.

## CONCLUSIONS

It is imperative to treat wastewater containing MB dye before discharging it into the environment because of its detrimental effects on water quality. In this study, we synthesized CaO/AC/ZnO nanocomposite from biomaterial waste by adding activated carbon from date palm seeds with calcium oxide from eggshells and ZnO nanoparticles to the nanocomposite. The nanoparticles were then used to study the photodegradation of methylene blue (MB) under visible light. The physical features of all the adsorbents (AC, CaO, AC/ZnO, and CaO/AC/ZnO nanocomposite) were studied through FT-IR, XRD, SEM, BET, and TEM analyses. The results showed that the optimized conditions for composites of the MB of degradation were a pH of 9, irradiation time were at 100 minutes, MB concentration of 5 mg/L, and a photocatalyst quantity of 2.5 g/L. The findings demonstrated the mesoporous structure and excellent sorption capabilities of the CaO/AC/ZnO nanocomposite. Furthermore, during 100 minutes of sunshine irradiation, the photodegradation efficiency of MB utilizing AC, CaO, AC/ZnO, and CaO/AC/ZnO nanocomposite was 33.23, 37.58, 54.61, and 88.92%, respectively. This suggests that enhancing the surface characteristics of the AC boosts photodegradation efficiency. After 120 minutes of sun exposure, the CaO/AC/ZnO nanocomposite's MB removal effectiveness was 96.7%. As a result, the CaO/AC/ZnO nanocomposite exhibits promise as an effective, versatile photocatalyst for the photodegradation of MB dyes in wastewater.

### Declarations

**Conflict of interest:** The authors declare no competing interests.

### REFERENCE


[1] Sridevi, M., Nirmala, C., Jawahar, N., Arthi, G., Vallinayagam, S., Sharma, V.K; "Role of nanomaterial's as adsorbent for heterogeneous reaction in waste water treatment", J. Mol. Struct. 1241, 130596, 2021, doi: 10.1016/j.molstruc.2021.130596.

[2] Cheng et el., "Highly efficient removal of methylene blue dye from an aqueous solution using cellulose acetate nanofibrous membranes modified by polydopamine", ACS Omega. 5, 5389–5400, 2020, doi:10.1021/acsomega.9b04425.

[3] Khan at el," Review on methylene blue: its properties, uses, toxicity and photodegradation", Water (Switzerland), 14, 242, 2022, doi: 10.3390/w14020242.

[4] Shehzad at el., "TiO2/Activated Carbon/2D selenides composite photocatalysts for industrial wastewater Treatment", Water. 15, 1788, 2023, doi: 10.1007/978-981-16-4921-9_55-2.

[5] Santoso, E., Ediati, R., Kusumawati, Y., Bahruji, H., Sulistiono, D.O., Prasetyoko, D., "Review on recent advances of carbon based adsorbent for methylene blue removal from waste water", Mater. Today Chem, 16, 100233, 2020, doi:10.1016/j.mtchem.2019.100233.

[6] Amalina, F., Razak, A.S.A., Krishnan, S., Zularisam, A.W., Nasrullah, M," Dyes removal from textile wastewater by agricultural waste as an absorbent – A review", Clean. Waste Syst, 3, 100051, 2022, doi:10.1016/j.clwas.2022.100051

[7] Algethami, J.S., Hassan, M.S., Alorabi, A.Q., Alhemiary, N.A., Fallatah, A.M., Alnaam, Y., Almusabi, S., Amna, T," Manganese Ferrite–hydroxyapatite nanocomposite synthesis: biogenic waste remodeling for water decontamination. Nanomaterials", 12, ,2022, doi:10.3390/nano12101631.

[8] Zhong, F., Wang, P., He, Y., Chen, C., Li, H., Yu, H., Chen, J, " Preparation of stable and superior flux GO/LDH/PDA-based nanofiltration membranes through electrostatic self-assembly for dye purification", Polym. Adv. Technol. 30, 1644–1655, 2019, doi:10.1002/pat.4595.

[9] Naresh Yadav, D., Anand Kishore, K., Saroj, D, " A Study on removal of Methylene Blue dye by photo catalysis integrated with nanofiltration using statistical and experimental approaches," Environ. Technol, 42, 2968–2981, 2021, doi:10.1080/09593330.2020.1720303.

[10] Banat, F., Al-Asheh, S., Qtaishat, M, "Treatment of waters colored with methylene blue dye by vacuum membrane distillation. Desalination", 174, 87–96, 2005, doi:10.1016/j.desal.2004.09.004.

[11] Imron, M.F., Kurniawan, S.B., Soegianto, A., Wahyudianto, F.E, "Phytoremediation of methylene blue using duckweed (Lemna minor", Heliyon, 5, e02206, 2019, doi:10.1016/j.heliyon.2019.e02206.

[12] Mohamed, F., Shaban, M., Aljohani, G., Ahmed, A.M, " Synthesis of novel eco-friendly CaO/C photocatalyst from coffee and eggshell wastes for dye degradation", J. Mater. Res. Technol, 14, 3140–3149, 2021, dio:10.1016/j.jmrt.2021.08.055.

[13] Kim, S., Yu, M., Yoon, Y, "Fouling and retention mechanisms of selected cationic and anionic dyes in a $Ti_3C_2T$ x MXene-ultrafiltration hybrid system", ACS Appl. Mater, Interfaces. 12, 16557–16565, 2020, dio:10.1021/acsami.0c02454.

[14] Maroneze, M.M., Zepka, L.Q., Vieira, J.G., Queiroz, M.I., Jacob-Lopes, E, "The degradation of methylene blue dye by the strains of Pleurotus sp. with potential applications in bioremediation processes, Rev. Ambient. e Agua, 13, e2247, 2018, doi:10.4136/1980-993X.

[15] Tir, M., Moulai-Mostefa, N., Nedjhioui, M, 'Optimizing decolorization of methylene blue dye by electrocoagulation using Taguchi approach", Desalin. Water Treat, 55, 2705–2710, 2015, doi:10.1080/19443994.2014.940652.

[16] Lau, Y.-Y., Wong, Y.-S., Teng, T.-T., Morad, N., Rafatullah, M., Ong, S. A, "Degradation of cationic and anionic dyes in coagulation–flocculation process using bi-functionalized silica hybrid with aluminum-ferric as auxiliary agent", RSC Adv, 5, 34206–34215, 2015, doi:10.1039/C5RA01346A.

[17] García at el, "Microwave atmospheric pressure plasma jets for wastewater treatment: Degradation of methylene blue as a model dye", Chemosphere, 180, 239–246, 2017, doi:10.1016/j.chemosphere.2017.03.126.

[18] El-Ashtoukhy, E.-S.Z., Fouad, Y.O, "Liquid–liquid extraction of methylene blue dye from aqueous solutions using sodium dodecylbenzenesulfonate as an extractant", Alexandria Eng. J, 54, 77–81, 2015, doi:10.1016/j.aej.2014.11.007.

[19] Liu, L., He, D., Pan, F., Huang, R., Lin, H., Zhang, X, "Comparative study on treatment of methylene blue dye wastewater by different internal electrolysis systems and COD removal kinetics, thermodynamics and mechanism",Chemosphere, 238, 124671, 2020, doi:10.1016/j.chemosphere.2019.124671.

[20] Shahzad at el, "Versatile Ag2O and ZnO nanomaterials fabricated via annealed Ag-PMOS and ZnO-PMOS: An efficient photocatalysis tool for azo dyes", J. Mol. Liq, 356, 119036, 2022, doi:10.1016/j.molliq.2022.119036

[21] Nadikatla, S.K., Chintada, V.B., Gurugubelli, T.R., Koutavarapu, R, "Review of recent developments in the fabrication of zno/cds heterostructure photocatalysts for degradation of organic pollutants and hydrogen production", Molecules, 28, 4277, 2023, doi:10.3390/molecules28114277.

[22] Manikanika, Chopra, L., Kumar, R, "Photocatalytic degradation efficiencies of ZnO nanoparticles and $CeO_2$ nanosheets synthesized via combustion method", Bull. Mater. Sci, 46, 181, 2023, doi:10.1007/s12034-023-03028-9.

[23] Parambil, J.A., V.M, A.M., Karazhanov, S.Z., Peediyekkal, J, "Synthesis , Surface morphology , optical properties and photocatalyst activities of $TiO_2$ / ZnO / $Fe_2O_3$, Res. Sq. 1–11, 2020, doi:10.21203/rs.3.rs-70935/v1 License.

[24] Moosavi at el, "Application of efficient magnetic particles and activated carbon for dye removal from wastewater", ACS Omega, 5, 20684–20697, 2020, doi:org/10.1021/acsomega.0c01905.

[25] Narasimharao at el," $Fe_3O_4$@date seeds powder: A sustainable nanocomposite material for wastewater treatment", J. Mater. Res. Technol, 18, 3581–3597, 2022, doi:10.1016/j.jmrt.2022.03.176.

[26] Yuvaraja at el, "Removal of U(VI) from aqueous and polluted water solutions using magnetic Arachis hypogaea leaves powder impregnated into chitosan macromolecule", Int. J. Biol. Macromol, 148, 887–897, 2020, doi:10.1016/j.ijbiomac.2020.01.042.

[27] Podder, M.S., Majumder, C.B, "Sequestering of As(III) and As(V) from wastewater using a novel neem leaves/$MnFe_2O_4$ composite biosorbent", Int. J. Phytoremediation,18, 1237–1257, 2016, doi:10.1080/15226514.2016.1193467.

[28] Banerjee, S.S., Chen, D.-H, "Fast removal of copper ions by gum arabic modified magnetic nano-adsorbent", J. Hazard. Mater, 147, 792–799, 2007, doi:10.1016/j.jhazmat.2007.01.079.

[29] Cai, Y., Shen, Y., Xie, A., Li, S., Wang, X, "Green synthesis of soya bean sprouts-mediated superparamagnetic $Fe_3O_4$ nanoparticles", J. Magn. Magn. Mater, 322, 2938–2943, 2010, doi:10.1016/j.jmmm.2010.05.009.

[30] Choudhry, A., Sharma, A., Khan, T.A., Chaudhry, S.A, "Flax seeds based magnetic hybrid nanocomposite: An advance and sustainable material for water cleansing", J. Water Process Eng, 42, 102150, 2021, doi:10.1016/j.jwpe.2021.102150.

[31] Abdus-Salam, N., Ikudayisi-Ugbe, A. V., Ugbe, F.A, "Adsorption studies of acid dye – Eosin yellow on date palm seeds, goethite and their composite", Chem. Data Collect. 31, 100626, 2021, doi:10.1016/j.cdc.2020.100626.

]32] Altıntıg, E., Yenigun, M., Sarı, A., Altundag, H., Tuzen, M., Saleh, T.A, "Facile synthesis of zinc oxide nanoparticles loaded activated carbon as an eco-friendly adsorbent for ultra-removal of malachite green from water, Environ. Technol. Innov. 21, 101305, 2021, doi:10.1016/j.eti.2020.101305.

[33] Khaleghi, H., Esmaeili, H., Jaafarzadeh, N., Ramavandi, B, "Date seed activated carbon decorated with CaO and $Fe_3O_4$ nanoparticles as a reusable sorbent for removal of formaldehyde", Korean J. Chem. Eng, 39, 146–160, 2022, doi:10.1007/s11814-021-0972-4.

[34] Al-Shwyeh, H.A, "Date Palm (Phoenix dactylifera L.) Fruit as Potential Antioxidant and Antimicrobial Agents", J. Pharm. Bioallied Sci, 11, 1–11, 2019, doi:10.4103/jpbs.JPBS_168_18

[35] El- Habba, M.S., Al- Mulhim, F, "The competitiveness of the Saudi Arabian date palm: An analytical study", African J. Agric. Res, 8, 5260–5267, 2013, doi:10.5897/AJAR2013.6861

[36] Ansari, M.A, "One-Pot Facile Green Synthesis of Silver Nanoparticles Using Seed Extract of Phoenix dactylifera and Their Bactericidal Potential against MRSA", Evidence-Based Complement. Altern. Med, ID 1860280, 1–9, 2018, doi:10.1155/2018/1860280

[37] Hassan, A.F., Hrdina, R, 'Chitosan/nanohydroxyapatite composite based scallop shells as an efficient adsorbent for mercuric ions: Static and dynamic adsorption studies, Int. J. Biol. Macromol, 109, 507–516, 2018, doi:10.1016/j.ijbiomac.2017.12.094

[38] Alazmi, A., Nicolae, S.A., Modugno, P., Hasanov, B.E., Titirici, M.M., Costa, P.M.F.J, "Activated carbon from palm date seeds for $CO_2$ capture, Int. J. Environ. Res. Public Health, 18, 2021, doi:10.3390/ijerph182212142

[39] Seffati, K., Esmaeili, H., Honarvar, B., Esfandiari, N, "AC/$CuFe_2O4$@ CaO as a novel nanocatalyst to produce biodiesel from chicken fat. Renew, Energy, 147, 25–34, 2020, doi:10.1016/j.renene.2019.08.105

[40] Jalu, R.G., Chamada, T.A., Kasirajan, D.R.: Calcium oxide nanoparticles synthesis from hen eggshells for removal of lead (Pb(II)) from aqueous solution. Environ. Challenges. 4, 100193 (2021). https://doi.org/10.1016/j.envc.2021.100193

[41] Elsayed, M.S., Ahmed, I.A., Bader, D.M.D., Hassan, A.F, 'Green synthesis of nano zinc oxide/nanohydroxyapatite composites using date palm pits extract and eggshells: Adsorption and photocatalytic degradation of methylene blue, Nanomaterials, 12, 2022, doi:10.3390/nano12010049

[42] Fong, W.M., Affam, A.C., Chung, W.C, 'Synthesis of Ag/Fe/CAC for colour and COD removal from methylene blue dye wastewater, Int. J. Environ. Sci. Technol, 17, 3485–3494, 2020, doi:10.1007/s13762-020-02720-1

[43] Iqbal, A., Ibrahim, N.H., Rahman, N.R.A., Saharudin, K.A., Adam, F., Sreekantan, S., Yusop, R.M., Jaafar, N.F., Wilson, L.D, 'ZnO Surface Doping to Enhance the Photocatalytic Activity of Lithium Titanate/$TiO_2$ for Methylene Blue Photodegradation under Visible Light Irradiation. Surfaces", 3, 301–318, 2020, doi:10.3390/surfaces3030022

[44] Rodrigues, S.C., Silva, M.C., Torres, J.A., Bianchi, M.L, 'Use of Magnetic activated carbon in a solid phase extraction procedure for analysis of 2,4-dichlorophenol in water samples", Water, Air, Soil Pollut, 231, 294, 2020, doi:10.1007/s11270-020-04610-1

[45] Stan, M., Popa, A., Toloman, D., Silipas, T.D., Vodnar, D.C, 'Antibacterial and antioxidant activities of ZnO nanoparticles synthesized using extracts of allium sativum, rosmarinus officinalis and ocimum basilicum, Acta Metall. Sin. (English Lett), 29, 228–236, 2016, doi:10.1007/s40195-016-0380-7

[46] Alamdari at el, "Preparation and characterization of zinc oxide nanoparticles using leaf extract of sambucus ebulus sanaz", Appl. Sci, 10, 1–19, 2020, doi:10.3390/app10103620

[47] Suprapto, Fauziah, T.R., Sangi, M.S., Oetami, T.P., Qoniah, I., Prasetyoko, D, "Calcium oxide from limestone as solid base catalyst in transesterification of Reutealis trisperma oil",Indones. J. Chem, 16, 208–213, 2016, doi:10.22146/IJC.21165

[48] Basak, M., Rahman, M.L., Ahmed, M.F., Biswas, B., Sharmin, N, 'The use of X-ray diffraction peak profile analysis to determine the structural parameters of cobalt ferrite nanoparticles using Debye-Scherrer, Williamson-Hall, Halder-Wagner and Size-strain plot: Different precipitating agent approach, J. Alloys Compd, 895, 162694, 2022, doi:10.1016/j.jallcom.2021.162694

[49] Taha, A., Aissa, M. Ben, "Green Synthesis of an Activated Carbon-Supported Ag and ZnO Nanocomposite for Photocatalytic

Degradation and Its Antibacterial Activities. Molecules", 25, 1586, 2020, doi:10.3390/molecules25071586

[50] Zhang, L., Zhang, M., You, S., Ma, D., Zhao, J., Chen, Z, "Effect of $Fe^{3+}$ on the sludge properties and microbial community structure in a lab-scale $A_2O$ process", Sci. Total Environ, 780, 146505, 2021, doi: 10.1016/j.scitotenv.2021.146505

[51] Wang at el, "Preparation and Characterization of CaO/ZnO Core-shell Structured Nanoparticles", Chem. Res. Chinese Univ, 36, 970–975, 2020, doi:10.1007/s40242-020-9029-1

[52] Zhao, H., Zhang, M, "Research progress of CaO-based absorbents prepared from different calcium sources", IOP Conf. Ser. Earth Environ. Sci, 474, 2020, doi:10.1088/1755-1315/474/5/052058

[53] Daud, N.K., Muthiyah, D, "Adsorption of $CO_2$ on Activated Carbon, Fe-Based Metal Organic Framework, ZnO, and CaO for Carbon Capture and Storage Application", Chem. Eng. Technol, 46, 2469–2479, 2023, doi: 10.1002/ceat.202200552

[54] Azeez at el, "The effect of surface charge on photocatalytic degradation of methylene blue dye using chargeable titania nanoparticles", Sci. Rep, 8, 1–9, 2018, doi:10.1038/s41598-018-25673-5

[55] Saeed, K., Zada, N., Khan, I., Sadiq, M, "Synthesis, characterization and photodegradation application of Fe-Mn and F-MWCNTs supported Fe-Mn oxides nanoparticles, Desalin. Water Treat, 108, 362–368, 2018, doi: 10.5004/dwt.2018.22010

[56] Nazriati, Maknun, L., Fajaroh, F, "Removal methylene blue from aqueous solution using silica aerogel prepared from bagasse ash", IOP Conf. Ser. Earth Environ. Sci, 299, 2019, dio:10.1088/1755-1315/299/1/012044

[57] Zafisah, N.S., Ang, W.L., Mohammad, A.W, "Cake filtration for suspended solids removal in digestate from anaerobic digested palm oil mill effluent (pome), Water Conserv. Manag, 2, 5–9, 2018, doi:10.26480/wcm.01.2018.05.09

[58] Salama, A., Mohamed, A., Aboamera, N.M., Osman, T.A., Khattab, A, "Photocatalytic degradation of organic dyes using composite nanofibers under UV irradiation", Appl. Nanosci, 8, 155–161, 2018, doi: 10.1007/s13204-018-0660-9

[59] Abdellah, M.H., Nosier, S.A., El-Shazly, A.H., Mubarak, A.A, "Photocatalytic decolorization of methylene blue using $TiO_2$/UV system enhanced by air sparging", Alexandria Eng. J, 57, 3727–3735, 2018, doi: 10.1016/j.aej.2018.07.018

[60] Gorzin, F., Bahri Rasht Abadi, M.M, "Adsorption of Cr(VI) from aqueous solution by adsorbent prepared from paper mill sludge: Kinetics and thermodynamics studies", Adsorpt. Sci. Technol, 36, 149–169, 2018, doi: 10.1177/0263617416686976

[61] Li, B., Wu, H., Zhang, C., Zheng, W., Sun, D., Lei, S," Dual functional Fe/AC for treating phenol solutions by adsorption coupled with dry catalytic oxidation technology", Desalin. Water Treat, 165, 148–162, 2019, doi:10.5004/dwt.2019.24579

[62] Khade, G. V, Gavade, N.L., Suwarnkar, M.B., Dhanavade, M.J., Sonawane, K.D., Garadkar, K.M," Enhanced photocatalytic activity of europium doped $TiO_2$ under sunlight for the degradation of methyl orange", J. Mater. Sci. Mater. Electron, 28, 11002–11011,2017, doi: 10.1007/s10854-017-6883-9

[63] Fito at el, "Adsorption of methylene blue from textile industrial wastewater using activated carbon developed from rumex abyssinicus plant, Sci. Rep, 13, 1–17, 2023, doi: 10.1038/s41598-023-32341-w

[64] Park, H., Choi, W," Photocatalytic Reactivities of nafion-coated $TiO_2$ for the degradation of charged organic compounds under UV or visible light", J. Phys. Chem. B, 109, 11667–11674, 2005, doi:10.1021/jp051222s

[65] Raizada, P., Shandilya, P., Singh, P., Thakur, P," Solar light-facilitated oxytetracycline removal from the aqueous phase utilizing a $H_2O_2$/$ZnWO_4$/CaO catalytic system", J. Taibah Univ. Sci, 11, 689–699, 2017, doi:10.1016/j.jtusci.2016.06.004

[66] Singh, D.K., Pandey, D.K., Yadav, R.R., Singh, D, "A study of nanosized zinc oxide and its nanofluid", Pramana - J. Phys, 78, 759–766, 2012, doi:10.1007/s12043-012-0275-8

DOI: https://doi.org/10.15379/ijmst.v11i1.3625